Mn-Doped RuO_2 Nanocrystals with Abundant Oxygen Vacancies for Enhanced Oxygen Evolution in Acidic Media

Caixia Zheng[ab],Bing Huang[a], Xuwei Liu[a], Hao Wang[ab], Lunhui Guan[ab]*

[a] *CAS Key Laboratory of Design and Assembly of Functional Nanostructures, Fujian Key Laboratory of Nanomaterials, Fujian Institute of Research on the Structure of Matter, Chinese Academy of Sciences, Fuzhou 350108, China.*
[b] *School of Chemistry, Fuzhou University, Fuzhou 350108, China.*

*Corresponding author. guanlh@fjirsm.ac.cn

Electronic Supplementary Information (ESI) available: [details of any supplementary information available should be included here]. See DOI: 10.1039/x0xx00000x

Experimental Procedures

Synthesis of Mn-HMT: First, 2803.6mg of hexamethylenetetramine (HMT) and 125.84mg of $MnCl_2$ were dissolved in 50ml and 30ml of ethanol, respectively. Then stir at room temperature for 1 hour until completely dissolved (if the HMT is not completely dissolved, add 2ml water). $MnCl_2$ was slowly dropped into HMT, stirred for 2 hours, and then centrifuged 3 times with isopropanol as a cleaning agent to collect the precipitate (Centrifuge speed set to 7500r/min, centrifuge time is 5 minutes). Finally, the samples were dried using a vacuum freeze dryer.

Synthesis of MnRu-HMT-120: Take the prepared Mn-HMT (120mg) and dissolve it in 5ml tetrahydrofuran. 120mg$RuCl_3$•$3H_2O$(Admas) was dissolved in 1ml tetrahydrofuran. They were ultrasounded for 15 minutes. $RuCl_3$•$3H_2O$ is then slowly dripped into MnRu-HMT and stirred for 24h. The final sample was collected by two times. When centrifuging, tetrahydrofuran is used as cleaning agent, and the centrifuge speed is 10000r/min. The centrifuge time is 10 minutes. Finally, the samples were dried using a vacuum freeze dryer.

Synthesis of MnRu-HMT-X:X stands for weighing X mg $RuCl_3$•$3H_2O$. The remaining steps are exactly the same as above.

Synthesis of Mn-RuO_2-120($NaNO_3$): 70mg of MnRu-HMT-120 was mixed with 2100mg of $NaNO_3$. After they are fully ground into a fine powder, they are sintered in a tube furnace at 350 ° C for 2 hours, and after cooling, the final sample is obtained by pumping and filtering. Finally, the samples were dried using a vacuum freeze dryer.

Synthesis of Mn-RuO_2-X($NaNO_3$): Except for taking a different MnRu-HMT-X precursor, the remaining steps are exactly the same as above.

Synthesis of Mn-RuO_2-120: The prepared 70mg MnRu-HMT-120 was taken and sintered in a tube furnace at 350℃ for 2 hours. After cooling, the final sample was obtained by pumping and filtering. Finally, the samples were dried using a vacuum freeze dryer.

Synthesis of Mn-RuO_2-X: Except for taking a different MnRu-HMT-X precursor, the remaining steps are exactly the same as above.

Experimental Procedures: The X-ray diffraction patterns were recorded using a Rigaku Miniflex 600 equipped with a Cu Kα X-ray source (λ=0.154 nm). The morphology of the catalyst was analyzed by emission scanning electron microscopy (SEM, em-30+, FEI Nova Nano-SEM 230). The microstructure of the catalyst was analyzed by high-resolution transmission electron microscopy (HR-TEM, FEI Talos-F200S) and spherical-aberration-corrected high-angle annular dark-field scanning transmission electron microscopy (HAADF-STEM, JEM-ARM300F). X-ray photoelectron spectroscopy (XPS) spectra were obtained using a ThermoFisher ESCALAB 250Xi and calibrated to the adventitious C1s peak at 284.8 eV. X-ray absorption spectra (XAS) were collected at the Shanghai Synchrotron Radiation Facility (SSRF) beamline BL14W in transmission geometry and analyzed using Athena software. The concentrations of Mn and Ru on the catalyst were evaluated by inductively coupled plasma-atomic emission spectrometer (ICP-AES, Perkin Elmer Avio200).

Electrochemical tests: A three-electrode configuration with an RDE electrode was used to record the electrochemical data. The Ag/AgCl and Pt foil were employed as the reference and counter electrode, respectively. The ink was prepared by dispersing 5 mg samples into 970 μL isopropanol and 30 μL Nafion ionomer (D521, 5%wt). The coated amounts of samples depend on their Ru contents, and the amounts of the coated Ru in the RDE were 0.25 mg cm^{-2} for all samples. In RED, the coating amount of Ru in commercial RuO_2 is 0.29 mg cm^{-2}. Before data recording, N_2 was pumped into the electrolyte to remove O_2. Cyclic voltammetry curves at a scan rate of 100 mV s^{-1} between 1.1-1.2 V were performed for 30 min to stabilize the catalyst. LSV curves were then recorded at a scan rate of 5 mV s^{-1} to minimize the capacitive currents. The chronopotentiometry test was conducted on a Ti felt electrode with 0.53 mg cm^{-2} (Mn-RuO_2-120($NaNO_3$)) at 10 mA cm^{-2}.

PEMWE tests:

A home-built PEMWE was employed in this experiment. The plates were made of pure Ti metal and engraved with serpent-flow channels. The membrane electrode assemblies

(MEA) with an effective area of 2 cm^2 were fabricated by a spry-coating method. The loading capacity of Pt/C (40wt %, Tanaka) as cathode is 0.33 mg cm^{-2}. The loading capacity of catalyst (Mn-RuO_2-120($NaNO_3$)) as anode is 2.1 mg cm^{-2}. The loading capacity of commercial RuO_2 as cathode is 2.4 mg cm^{-2}. The ionomer (Nafion D521) contents used were 0.2 in the anode catalyst layers and 0.2 in the cathode catalyst layer. The porous layer for the cathode was a carbon paper with a 190 μm substrate and a 30 μm microporous layer, while the anode was Ti felts. The coated membrane was hot-pressed at 5 MPa and 130 ℃ for 5 minutes, sandwiched between Ti felt and a carbon paper. Pure water preheated to 80 ℃ was fed to the anode side only, and the plates were heated to 80 ℃ using two heating rods. Data recording was achieved using a calibrated Gamry interface 5000E potentiostat. The EIS spectra were measured at 1 V to determine the HFR. The polarization curves were obtained by sweeping the voltage from 0.9 V to 2.2 V at a scan rate of 5 mV s^{-1}.

DFT calculations:

The RuO_2 (110) surface selected for computation comprises three layers of Ru, with each unit cell encompassing 4 Ru atoms along its edges. The structure includes three substrates with a vacuum layer of 15 Å. All the structures were fully optimized in the mixed Gaussian and plane-wave code CP2K,[1] using the TZVP-MOLOPT basis set in combination with Geodecker–Teter–Hutter pseudopotentials and a plane-wave cut-off of 400 Ry with Grimme's D3 dispersion correction.[2]

Non-concerted proton-electron transfer and concerted proton-electron transfer:

For a coupled proton-electron transfer process：$M\text{□}H_2O \rightarrow M\text{□}OH + H^+ + e^-$

$$E_{SHE} = E_0 + \frac{RT}{F}\ln\left(\frac{\theta_{OH}a_{H^+}}{\theta_{H_2O}}\right) = E_0 + \frac{RT}{F}\ln\left(\frac{\theta_{OH}}{\theta_{H_2O}}\right) - 2.303\frac{RT}{F}pH \quad (1\text{-}1)$$

E_{RHE} ,

$$E_{RHE} = E_{SHE} + 2.303\frac{RT}{F}pH \quad (1\text{-}2)$$

$$E_{RHE} = E_0 + \frac{RT}{F}\ln\left(\frac{\theta_{OH}}{\theta_{H_2O}}\right) \quad (1\text{-}3)$$

E_0 , E_{SHE} , E_{RHE} , θ_{OH} , θ_{H_2O} and a_{H^+}, represent the thermodynamic equilibrium potential, the equilibrium potential relative to the hydrogen standard electrode, the equilibrium potential relative to the reversible hydrogen electrode, the coverage of -OH groups on the surface, the coverage of -H_2O on the surface, and the activity of hydrogen ions, respectively.

$$\frac{\partial E_{SHE}}{\partial pH} = -2.303\frac{RT}{F} = -59\ mV\ pH^{-1} \tag{1-4}$$

$$\frac{\partial E_{RHE}}{\partial pH} = 0\ mV\ pH^{-1} \tag{1-5}$$

For a non-coupled proton-electron transfer process: $M\square H_2O \rightarrow M\square OH + H^+ + xe^- (x < 1)$

$$E_{SHE} = E_0 + \frac{RT}{xF}\ln\left(\frac{\theta_{OH}a_{H^+}}{\theta_{H_2O}}\right) = E_0 + \frac{RT}{F}\ln\left(\frac{\theta_{OH}}{\theta_{H_2O}}\right) - 2.303\frac{RT}{xF}pH \tag{1-6}$$

$$E_{RHE} = E_{SHE} + 2.303\frac{RT}{F}pH \tag{1-7}$$

$$\frac{\partial E_{SHE}}{\partial pH} = -2.303\frac{RT}{xF} = -\frac{59}{x}\ mV\ pH^{-1} \tag{1-8}$$

$$\frac{\partial E_{RHE}}{\partial pH} = -59\left(1 - \frac{1}{x}\right) mV\ pH^{-1} \tag{1-9}$$

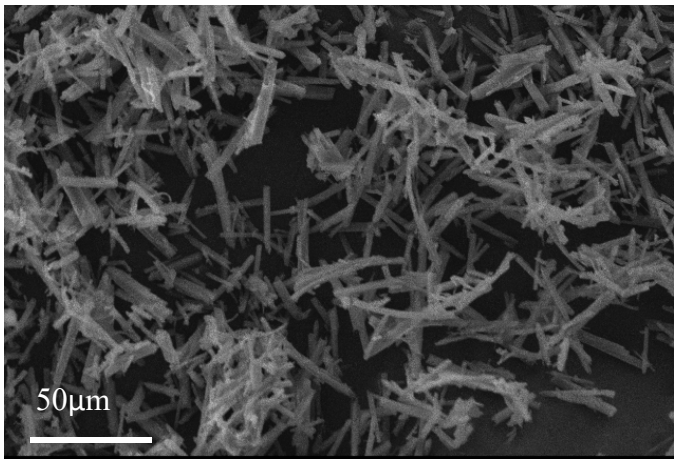

Figure S1. The SEM image of Mn-MHT.

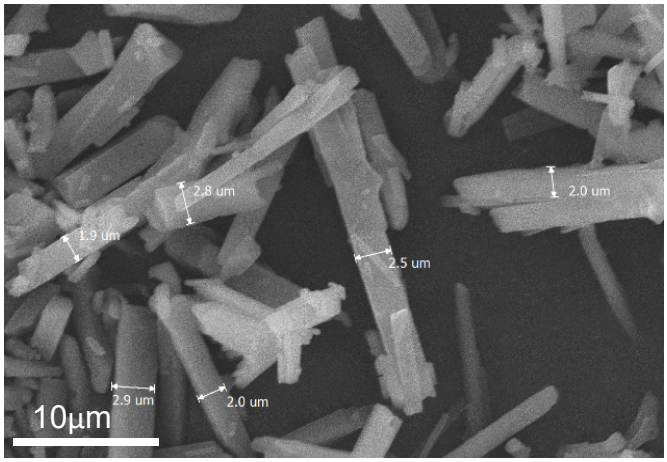

Figure S2. The SEM images of Mn-MHT showed that the average particle size was 2.35µm.

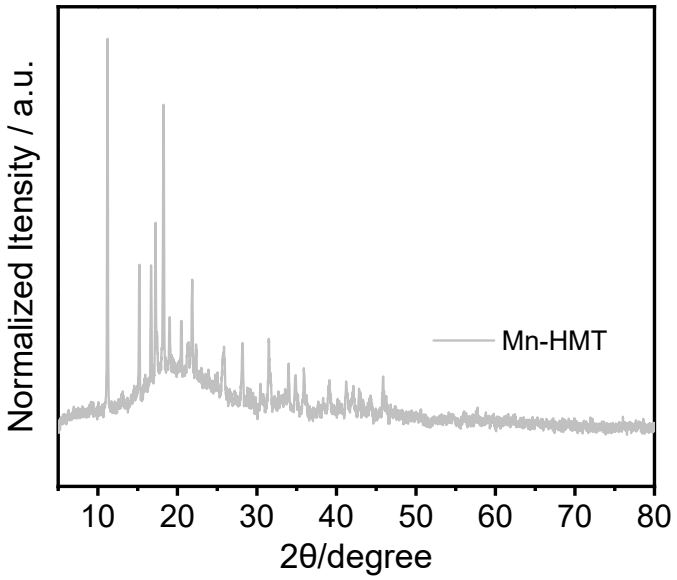

Figure S3. The XRD spectra of Mn-HMT.

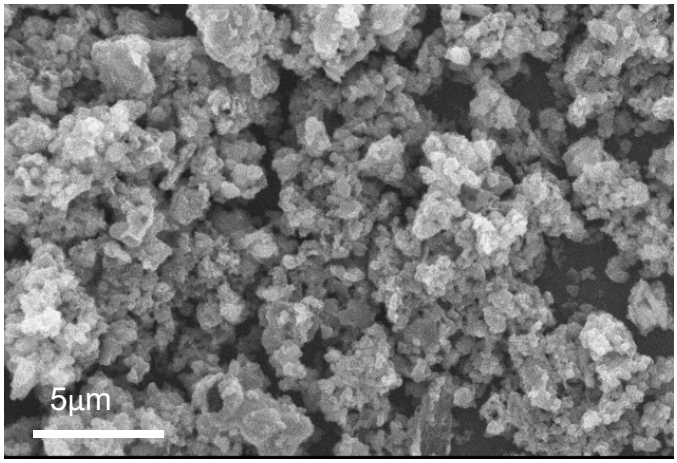

Figure S4. The SEM image of RuMn-MHT-120.

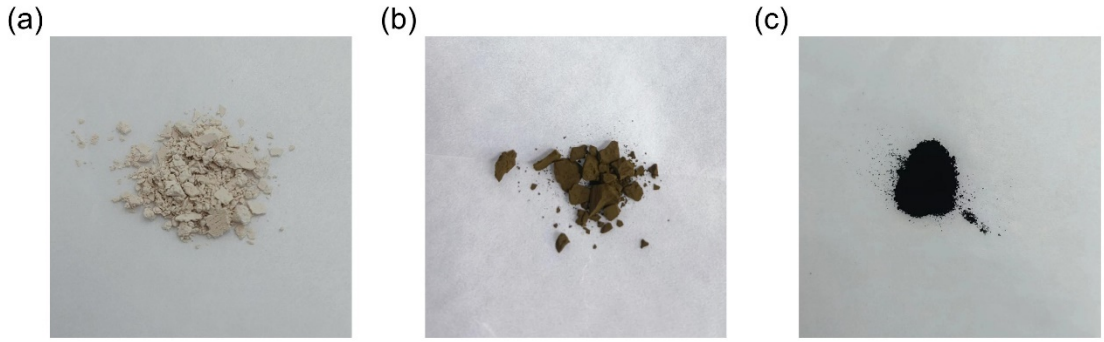

Figure S5. (a) The actual color of Mn-HMT. (b) The actual color of RuMn-HMT-120. (c) The actual color of Mn-RuO_2-120($NaNO_3$).

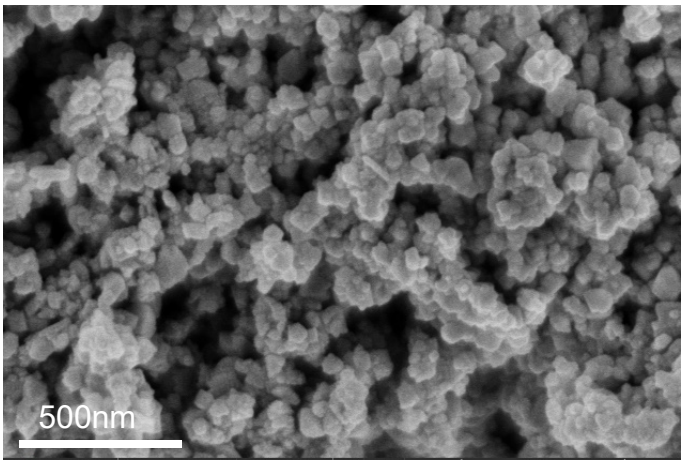

Figure S6. The SEM image of Mn-RuO_2-120($NaNO_3$).

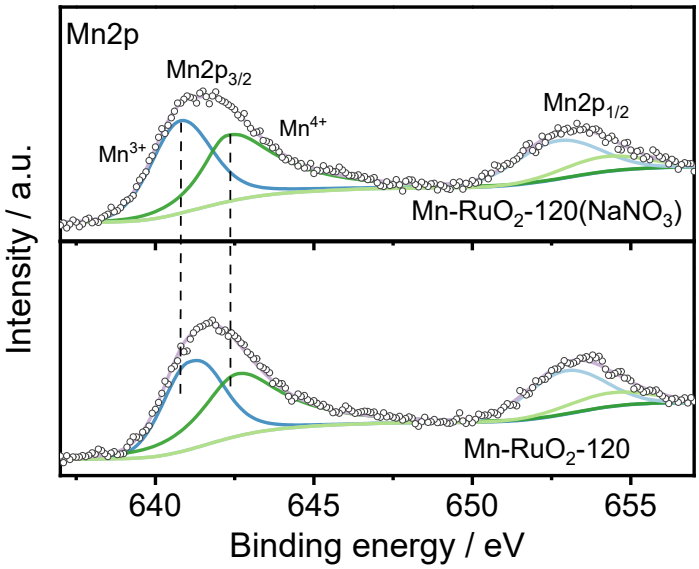

Figure S7. The Mn2P XPS profiles of Mn-RuO_2-120($NaNO_3$) and Mn-RuO_2-120.

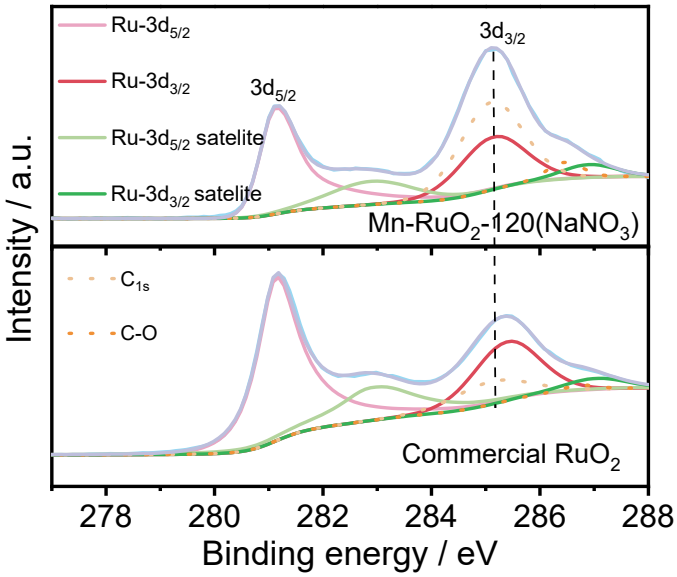

Figure S8. The Ru3d XPS profiles of Mn-RuO_2-120($NaNO_3$) and commercial RuO_2.

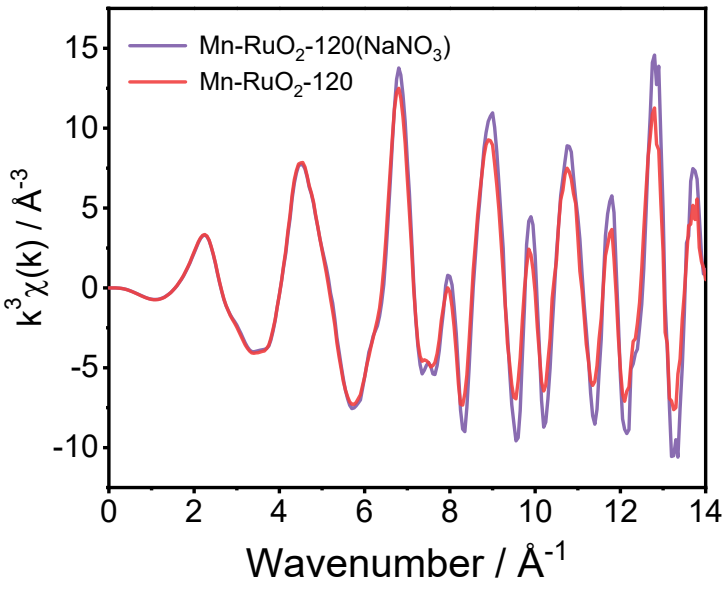

Figure S9 The k^3-weighted EXAFS spectra of the pristine Mn-RuO_2-120($NaNO_3$) and Mn-RuO_2-120.

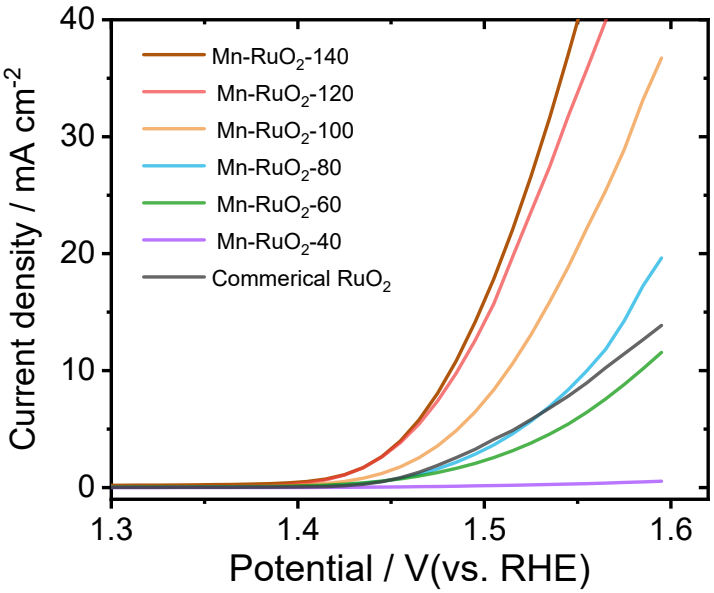

Figure S10. Gradient experiment: the LSV curve of Mn-RuO_2-X and commercial RuO_2.

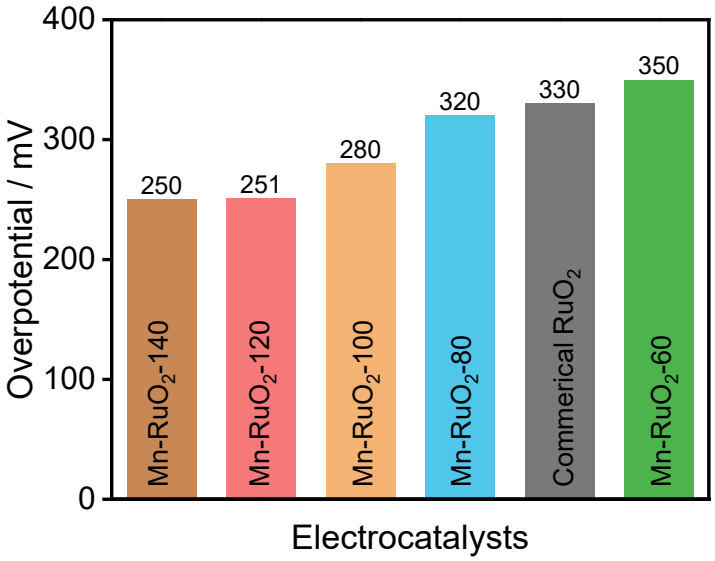

Figure S11. Gradient experiment: the η_{10} Statistical chart of Mn-RuO_2-X and commercial RuO_2.

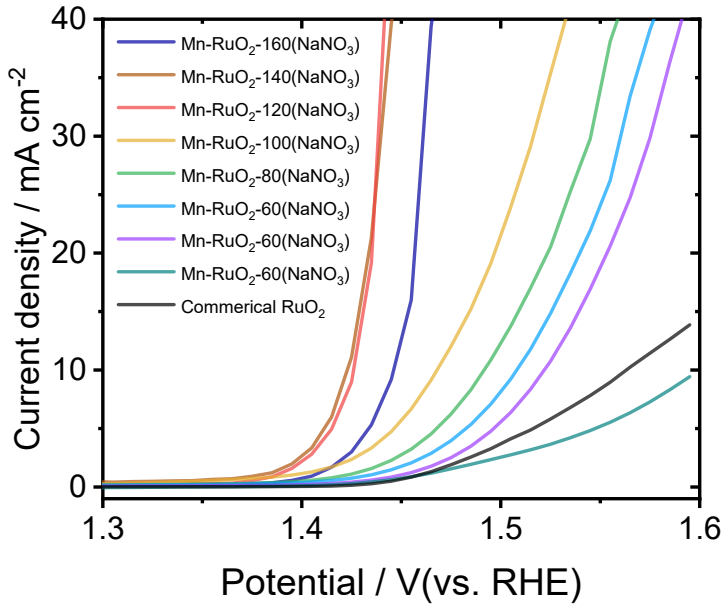

Figure S12. Gradient experiment: the LSV curve of Mn-RuO_2-X($NaNO_3$) and commercial RuO_2.

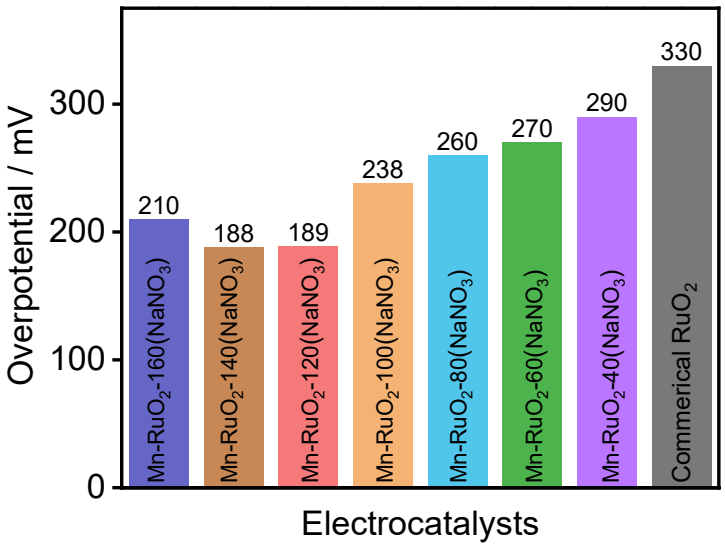

Figure S13. Gradient experiment: the η_{10} Statistical chart of Mn-RuO_2-X($NaNO_3$) and commercial RuO_2.

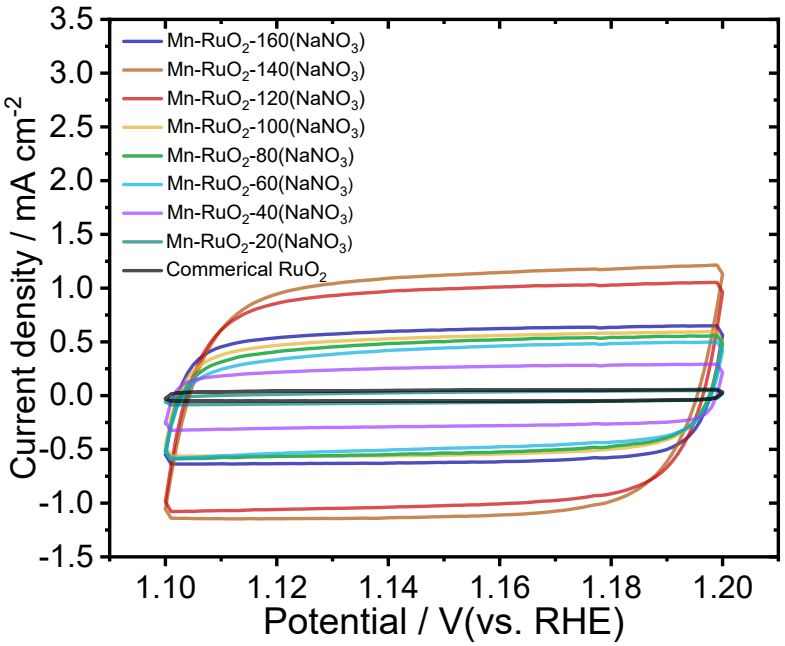

Figure S14. Gradient experiment: The ECSA of Mn-RuO_2-X($NaNO_3$) and commercial RuO_2.

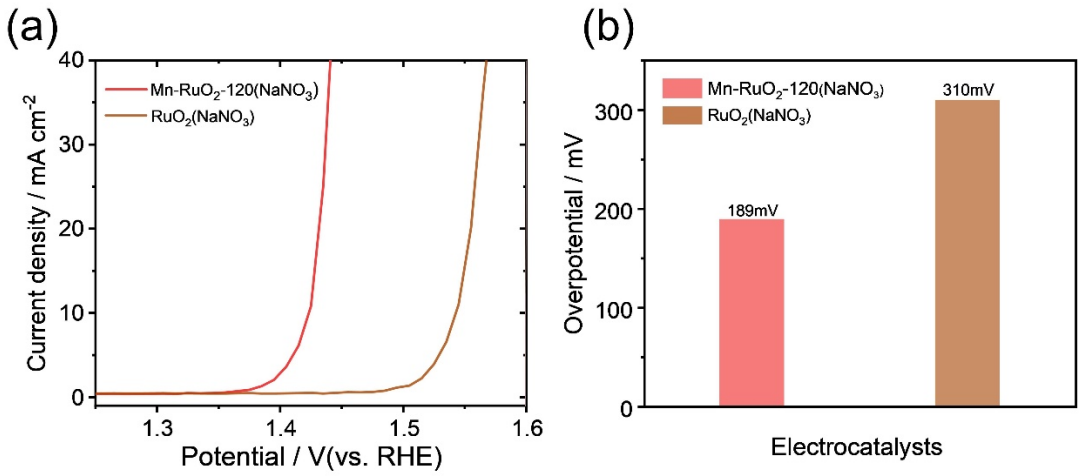

Figure S15. (a) The LSV curves picture of Mn-RuO_2-120($NaNO_3$) and RuO_2($NaNO_3$). (b) The η_{10} statistical chart of Mn-RuO_2-X and RuO_2($NaNO_3$).

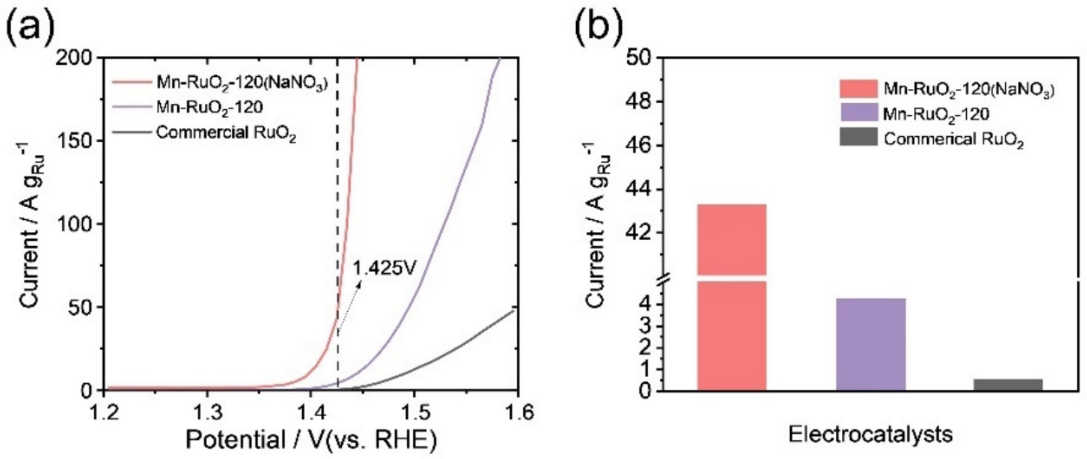

Figure S16. (a) The curve graph for Ru mass load normalized activity of Mn-RuO_2-120($NaNO_3$), Mn-RuO_2-120 and commercial RuO_2. (b) The Ru mass load normalized activity of Mn-RuO_2-120($NaNO_3$), Mn-RuO_2-120 and commercial RuO_2 in 1.425V（VS. RHE）.When operating at 1.425V (vs. RHE), the Ru mass load normalized activities for Mn-RuO_2-120($NaNO_3$), Mn-RuO_2-120, and commercial RuO_2 are 43.27A/g_{Ru}, 4.28 A/g_{Ru}, 0.51 A/g_{Ru}., respectively.

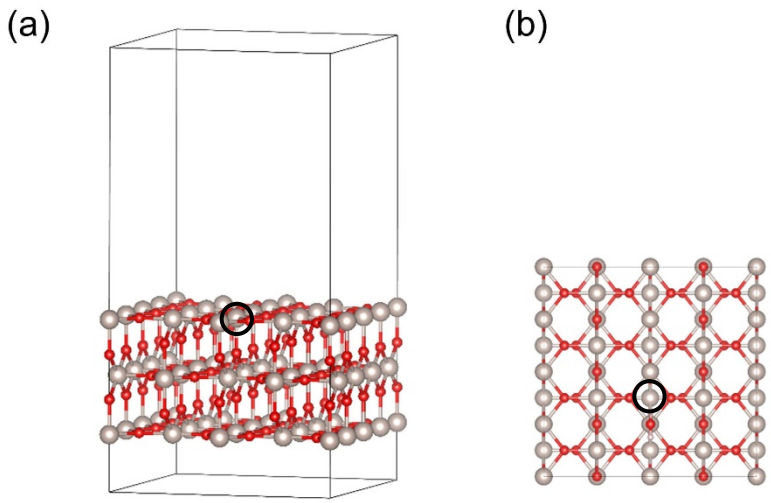

Figure S17. (a) Model 1 (the perfect RuO_2(110) surface). (b) The top view of the Model 1 (the perfect RuO_2(110) surface). The atom circled by dotted line represents the active site of Ru.

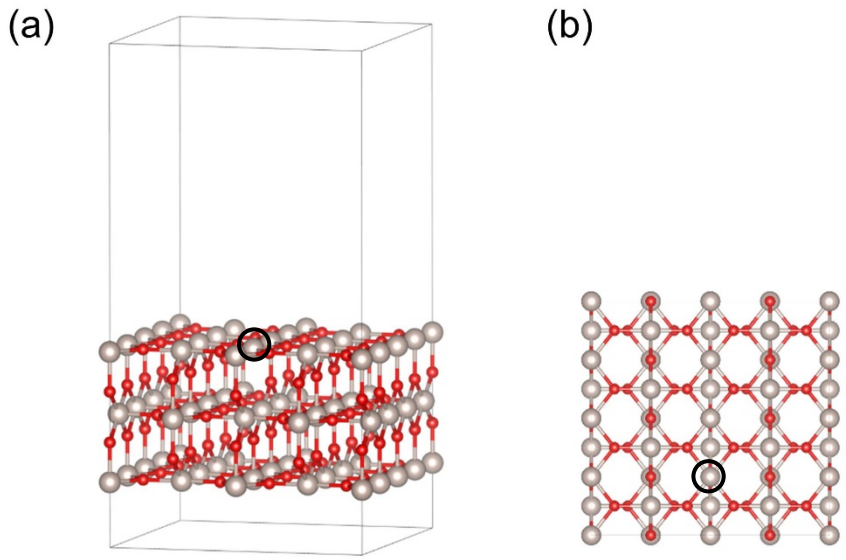

Figure S18. (a) Model 2 (RuO_2(110) surface with oxygen vacancy near adsorption site) (b) The top view of the Model 2 (RuO_2(110) surface with oxygen vacancy near adsorption site). The atom circled by dotted line represents the active site of Ru.

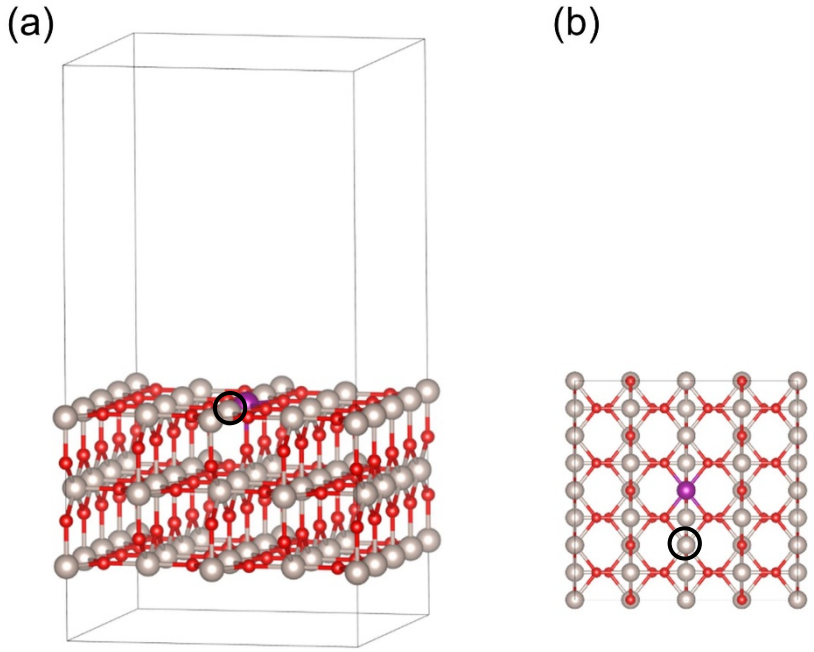

Figure S19. (a) Model 3 (Mn-doped RuO_2(110) surface with oxygen vacancy near adsorption site) (b) The top view of the Model 3 (Mn-doped RuO_2(110) surface with oxygen vacancy near adsorption site). The atom circled by dotted line represents the active site of Ru. The purple ball is the Mn atom.

Table S1. The elemental weight ratios from ICP-AES.

Samples	Ru(wt%)	Mn(wt%)
Mn-RuO_2-120($NaNO_3$)	59.7	15.6
Mn-RuO_2-100($NaNO_3$)	50.9	20.8
Mn-RuO_2-80($NaNO_3$)	38.4	28.3
Mn-RuO_2-60($NaNO_3$)	32	33.9
Mn-RuO_2-40($NaNO_3$)	20.7	43.5

Table S2. The Catalysts of mass loading.

Samples	Loading amount (mg $cm^{-2)}$	References
UfD-RuO_2	0.52	*Adv. Energy Mater.*[3]
$Cr_{0.6}Ru_{0.4}O_2$	0.283	*Nat. Commun.*[4]
H-RuO_2	0.191	*ACS Catal.*[5]
$RuNi_2$@G-250	0.32	*Adv. Mater.*[6]
Ni- RuO_2	0.40	*Nat. Mater.*[7]
Cu-doped RuO_2	0.275	*Adv. Mater.*[8]
Ru_3MoCeO_x	0.30	*Appl. Catal. B*[9]
Mn-RuO_2-120($NaNO_3$)	0.25	This work

Table S3. The previous reports related to Ru OER.

Samples	Electrolytes	η_{10}(mV)	References
Amorphous RuO_2	0.1 M $HClO_4$	205	*Angew. Chem. Int. Ed*. **2021**, 60, 18821-18829
RuO_2/$(Co,Mn)_3O_4$	0.5 M H_2SO_4	270	*Appl. Catal. B* **2021**, 297.
PtCo–RuO_2/C	0.1 M $HClO_4$	212	*Energy Environ. Sci*. **2022**, 15, 1119-1130.
$Nd_{0.1}RuO_x$ on carbon cloth	0.5 M H_2SO_4	211	*Adv. Funct. Mater*. **2023**, DOI:10.1002/adfm.202213304.
RuO_2 Nanosheets	0.5 M H_2SO_4	199	*Energy Environ. Sci*. **2020**, 13, 5143-5151.
Re-doped RuO_2	0.1 M $HClO_4$	190	*Nat. Commun.***2023**, 14, 354.
Ru/Co-N-C	0.5 M H_2SO_4	232	*Adv. Mater.* **2022**, 34, 2110103.
Ru_1–Pt_3Cu	0.1 M $HClO_4$	280	*Nat. Catal.* **2019**, 2, 304-313**.**
S-$RuFeO_x$	0.1 M $HClO_4$	187	*Adv. Funct. Mater*. **2021,** 31, 2101405.
C-RuO2-RuSe	0.5 M H_2SO_4	212	*Chem 8*, **2022**, DOI:10.1016/j.chempr.2022.02.003
Ru/RuO_2−Co_3O_4	0.1 M $HClO_4$	226	*ACS Sustainable Chem. Eng*. **2023**, 11, 13, 5155-5163
Pt-doped RuO_2	0.5 M H_2SO_4	228	*Sci. Adv.* **2022**, 8, eabl9271.
Ni-RuO_2	0.5 M H2SO_4	214	*Nat.Mater*. **2023**, 22, 100.
Mn-RuO_2-120($NaNO_3$)	0.1 M $HClO_4$	189	This work

Table S4. The caculated free energies

	$2H_2O$	$*OH+H_2O$ $+H^++e^-$	$*O+ H_2O$ $+2H^++2e^-$	$*OOH$ $+3H^++3e^-$	$2O_2$ $+4H^++4e^-$
RuO_2	0	0.21	1.12	3.09	4.92
RuO_2 with Oxygen Vacancy	0	1.12	1.84	3.61	4.92
RuO_2 with Mn-doped and Oxygen Vacancy	0	0.46	1.77	3.43	4.92

Table S5. The PEMWE performances for Ru-based materials.

Anode catalysts	Cell voltage (V)	Stability	Reference
RuO_2-NS/CF	1.57 V@1 A cm^{-2}	1 A cm^{-2} @10 h	*Nano Energy.* **2021**, 88, 106276.
Y_2MnRuO_7	1.51 V @ 0.2 A cm^{-2}	0.2 A cm^{-2} for 24 h	*Nat. Commun.* **2023,** 14, 2010.
$Nd_{0.1}RuO_x$	1.595 V @ 0.05 A cm^{-2}	0.05 A cm^{-2} for 50 h	*Adv. Funct. Mater*. **2023**, 33, 2213304.
$Nb_{0.1}Ru_{0.9}O_2$	1.69 V @ 1 A cm^{-2}	0.3 A cm^{-2} for 100 h	*Joule.* **2023,** 7, 558-573.
S-RuO_2/ATO	1.51 V @ 1 A cm^{-2}	0.5 A cm^{-2} for 40 h	*Adv. Sci.* **2022**, 9, 2201654.
RuO_2/SnO_2-1.5X	1.61 V @ 1 A cm^{-2}	0.5 A cm^{-2} for 25 h	*Small* **2023**, 19, 231516.
RuO_2/Defect-TiO_2	1.74 V @ 1.5 A cm^{-2}	1.0 A cm^{-2} for 6 h	*ACS Catal*. **2022**, 12, 9437-9445.
Mn-RuO_2-120($NaNO_3$)	1.69 V @ 1 A cm^{-2}	0.5 A cm^{-2} for 90 h	This work

Reference

1. VandeVondele, M. Krack, F. Mohamed, M. Parrinello, T. Chassaing and J. Hutter, QUICKSTEP: Fast and accurate density functional calculations using a mixed Gaussian and plane waves approach, *Comp. Phys. Comm.*, 2005, **167**, 103-128.
2. S. Grimme, J. Antony, S. Ehrlich and H. Krieg, A consistent and accurate ab initio parametrization of density functional dispersion correction (DFT-D) for the 94 elements H-Pu, *J. Chem. Phys.*, 2010, **132**, 154104.
3. X. Wang, S. Xi, P. Huang, Y. Du, H. Zhong, Q. Wang, A. Borgna, Y.-W. Zhang, Z. Wang, H. Wang, Z. G. Yu, W. S. V. Lee and J. Xue, Pivotal role of reversible NiO_6 geometric conversion in oxygen evolution, *Nature*, 2022, **611**, 702-708.
4. S. Yuan, J. Peng, B. Cai, Z. Huang, A. T. Garcia-Esparza, D. Sokaras, Y. Zhang, L. Giordano, K. Akkiraju, Y. G. Zhu, R. Hübner, X. Zou, Y. Román-Leshkov and Y. Shao-Horn, Tunable metal hydroxide–organic frameworks for catalysing oxygen evolution, *Nat. Mater.*, 2022, **21**, 673-680.
5. K. Wang, Y. Wang, B. Yang, Z. Li, X. Qin, Q. Zhang, L. Lei, M. Qiu, G. Wu and Y. Hou, Highly active ruthenium sites stabilized by modulating electron-feeding for sustainable acidic oxygen-evolution electrocatalysis, *EnEnergy Environ. Sci.*, 2022, **15**, 2356-2365.
6. W. Sun, Y. Fang, G. Sun, C. Dai, Y. Liu, J. Zhang, Y. Zhu and J. Wang, Ruthenium-Manganese Solid Solution Oxide with Enhanced Performance for Acidic and Alkaline Oxygen Evolution Reaction, *Chem Asian J*, 2023, **18,** e202300440.
7. R. Ge, L. Li, J. Su, Y. Lin, Z. Tian and L. Chen, Ultrafine Defective RuO_2 Electrocatayst Integrated on Carbon Cloth for Robust Water Oxidation in Acidic Media, *Adv. Energy Mater.*, 2019, **9**, 190313.
8. Y. C. Lin, Z. Q. Tian, L. J. Zhang, J. Y. Ma, Z. Jiang, B. J. Deibert, R. X. Ge and L. Chen, Chromium-ruthenium oxide solid solution electrocatalyst for highly efficient oxygen evolution reaction in acidic media, *Nat. Commun.*, 2019, **10**, 162.
9. J. He, W. Chen, H. Gao, Y. Chen, L. Zhou, Y. Zou, R. Chen, L. Tao, X. Lu and S. Wang, Tuning hydrogen binding modes within RuO_2 lattice by proton and electron co-doping for active and stable acidic oxygen evolution, *ACS Catal.*, 2022, **2**, 578-594.